Mon. Not. R. Astron. Soc. **337,** 1091–1104 (2002)

Evolution and colours of helium-core white dwarf stars: the case of low-metallicity progenitors

A. M. Serenelli,[1★†] L. G. Althaus,[1★‡] R. D. Rohrmann[2★§] and O. G. Benvenuto[1★¶]

[1] *Facultad de Ciencias Astronómicas y Geofísicas de la Universidad Nacional de La Plata and Instituto Astrofísica La Plata (CONICET), Paseo del Bosque S/N, (1900) La Plata, Argentina*

[2] *Observatorio Astronómico, Universidad Nacional de Córdoba, Laprida 854, (5000) Córdoba, Argentina*

Accepted 2002 August 16. Received 2002 August 15; in original form 2002 April 26

ABSTRACT

The present work is designed to explore the evolution of helium-core white dwarf (He WD) stars for the case of metallicities much lower than the solar metallicity ($Z = 0.001$ and 0.0002). Evolution is followed in a self-consistent way with the predictions of detailed and new non-grey model atmospheres, time-dependent element diffusion and the history of the white dwarf progenitor. Reliable initial models for low-mass He WDs are obtained by applying mass-loss rates to a 1-$M_\odot$ stellar model in such a way that the stellar radius remains close to the Roche lobe radius. The loss of angular momentum caused by gravitational wave emission and magnetic stellar wind braking are considered. Model atmospheres, based on a detailed treatment of the microphysics entering the WD atmosphere (such as the formalism of Hummer–Mihalas to deal with non-ideal effects) and hydrogen line and pseudo-continuum opacities, enable us to provide accurate colours and magnitudes at both early and advanced evolutionary stages.

We find that most of our evolutionary sequences experience several episodes of hydrogen thermonuclear flashes. In particular, the lower the metallicity, the larger the minimum stellar mass for the occurrence of flashes induced by CNO cycle reactions. The existence of a mass threshold for the occurrence of diffusion-induced CNO flashes leads to a marked dichotomy in the age of our models. Another finding of this study is that our He WD models experience unstable hydrogen burning via PP nuclear reactions at late cooling stages as a result of hydrogen chemically diffusing inwards. Such PP flashes take place in models with very low metal content.

We also find that models experiencing CNO flashes exhibit a pronounced turn-off in most of their colours at $M_V \approx 16$. Finally, colour–magnitude diagrams for our models are presented and compared with recent observational data of He WD candidates in the globular clusters NGC 6397 and 47 Tucanae.

Key words: stars: atmospheres – stars: evolution – stars: fundamental parameters – stars: interiors – white dwarfs.

1 INTRODUCTION

Low-mass helium-core white dwarf (He WD) stars are thought to be the result of the evolution of certain close binary systems. Mass-transfer episodes in binary systems are required to form low-mass He WDs because an isolated star would need a time-scale much longer than the present age of the universe to reach a WD configuration with a helium-rich interior. Low-mass WDs have been detected in large surveys (Bragaglia et al. 1990; Bergeron, Saffer & Liebert 1992; Bragaglia, Renzini & Bergeron 1995; Saffer, Livio & Yungelson 1998) and represent an appreciable fraction of the total population of WD stars.

Since He WDs began to be found in numerous binary configurations (Marsh 1995; Marsh, Dhillon & Duck 1995; Lundgren

★E-mail: serenell@fcaglp.unlp.edu.ar (AMS); althaus@fcaglp.unlp.edu.ar (LGA); rohr@astroscu.unam.mx (RDR); obenvenu@fcaglp.unlp.edu.ar (OGB).

†Fellow of the Consejo Nacional de Investigaciones Científicas y Técnicas (CONICET), Argentina.

‡Member of the Carrera del Investigador Científico y Tecnológico, Consejo Nacional de Investigaciones Científicas y Técnicas (CONICET), Argentina.

§Postdoctoral Fellow of the IA-UNAM. Now at: Instituto de Astronomía, UNAM, AP 70-264, 04510 México DF, Mexico.

¶Member of the Carrera del Investigador Científico, Comisión de Investigaciones Científicas de la Provincia de Buenos Aires.

et al. 1996; Moran, Marsh & Bragaglia 1997; Orosz et al. 1999; van Kerkwijk et al. 2000), they have captured the attention of many researchers who have devoted much effort to their study. Recent works with the emphasis on the evolutionary properties of these stars include Benvenuto & Althaus (1998), Hansen & Phinney (1998), Driebe et al. (1998), Sarna, Ergma & Antipova (2000), Althaus, Serenelli & Benvenuto (2001a) and Serenelli et al. (2001). In particular, Althaus et al. (2001a) have explored their evolution in a self-consistent way with nuclear burning, time dependent element diffusion and the history of the WD progenitor. Althaus et al. (2001a) find that element diffusion induces thermonuclear hydrogen shell flashes in He WDs with stellar masses greater than $\approx 0.18\ M_{\odot}$. As a result, He WDs more massive than $0.18\ M_{\odot}$ are characterized by thin hydrogen envelopes and a fast evolution, while less massive He WDs evolve much more slowly. As shown by Althaus et al. (2001a), this behaviour solves the discrepancies between the spin-down ages of the millisecond pulsars B1855+09, PSR J0034–0534 and PSR J1012+5307 and the cooling ages of their He WD companions. The evolution of the Althaus et al. (2001a) stellar models in the colour–colour and in the colour–magnitude diagrams have been analysed by Serenelli et al. (2001) who find, on the basis of detailed non-grey model atmospheres, that the emergent spectrum of low-mass He WDs becomes bluer within time-scales of astrophysical interest when the effective temperature decreases below 4000 K. Because Serenelli et al. (2001) were interested in the late stages of He WD evolution, they did not attempt a detailed modelling of the emergent spectrum of these stars at high effective temperature stages.

Interestingly, He WDs have also been detected or inferred in open and globular clusters (Anderson et al. 1997; Landsman et al. 1997; Edmonds et al. 1999). More recently, Edmonds et al. (2001) have optically detected the He WD companion to a millisecond pulsar in 47 Tucanae. In addition, Taylor et al. (2001) have presented evidence for a sequence of He WD candidates in the globular cluster NGC 6397. A proper interpretation of the observations of He WDs in globular clusters requires evolutionary calculations for He WD progenitors with much lower metallicities than the solar one. In this regard, the present work is designed to extend the evolutionary calculations presented in Serenelli et al. (2001) to the case of low metallicities. In addition, the present calculations constitute an improvement over those presented in Serenelli et al. (2001). Here a more detailed treatment of the microphysics entering the WD model atmosphere than that presented in that work is considered, thus enabling us to derive accurate colours and magnitudes for He WDs at high effective temperatures where the effects of line broadening opacities are not negligible. Finally, a much more realistic treatment of mass-loss phases than that attempted in Althaus et al. (2001a) and Serenelli et al. (2001) is considered in the present study. Details concerning our atmosphere models, evolutionary code and mass-loss treatment are briefly described in Section 2. Results are presented in Sections 3 and 4 is devoted to making some concluding remarks.

2 COMPUTATIONAL DETAILS AND INPUT PHYSICS

In this section we describe the main characteristics and the input physics of both the model atmosphere and evolutionary codes. Computational details concerning calculation of pre-WD evolution are also presented.

2.1 Model atmosphere code

At low effective temperatures, WD cooling is sensitive to the treatment of the outer boundary condition. Thus, appropriate outer boundary conditions for the cooling He WD models are derived on the basis of detailed non-grey model atmospheres, as done in Serenelli et al. (2001). This is an important aspect as far as cool WD ages are concerned. Additionally, these model atmospheres allow us to provide a grid of colour indices and magnitudes for our evolving models. The model atmospheric structure is described at length in Rohrmann (2001). Briefly, it is based on the assumption of constant gravity, local thermodynamic equilibrium and plane-parallel geometry, and includes the hydrogen and helium species (zero metallicity). Energy transfer by radiation and convection is considered and a standard linearization technique is employed to solve the resulting equations. The following species are taken into account: H, H_2, e^-, H^-, H^+, H_2^+, H_3^+, He, He^+ and He^{++}. All relevant bound–free, free–free and scattering processes contributing to opacity have been included in our calculations. Up-to-date collision-induced absorptions (CIA opacities) owing to H_2–H_2, H_2–He and H–He collisions are taken from the cross-section calculations by Borysow, Jorgensen & Fu (2001), Jorgensen et al. (2000) and Gustafsson & Frommhold (2001), respectively. CIA represents a major source of opacity in the infrared and dominates the shape of the emergent spectrum at low effective temperatures. Broadband colour indices have been calculated using the optical $UBVRI$ and infrared $JHKL$ passbands of Bessell (1990) and Bessell & Brett (1988), respectively. We use the calibration constants as derived on the basis of the synthetic flux of the model ($T_{\rm eff} = 9400$ K, $\log g = 3.95$) calculated by Kurucz (1979) for Vega, rather than the constants of Bergeron, Ruiz & Leggett (1997) we employed in Serenelli et al. (2001).

In the present work, important improvements have been incorporated in our model atmospheres, which have enabled us to derive accurate colours and magnitudes for both early and advanced stages of the cooling. Specifically, hydrogen line opacities from the Lyman, Balmer and Paschen series and pseudo-continuum absorptions have been included in our calculations. Also, non-ideal effects in the computation of chemical equilibrium of mixed hydrogen and helium gases are accounted via the occupation formalism of Hummer & Mihalas (1988), together with a modified version of the optical simulation of Däppen, Anderson & Mihalas (1987) to assess opacities in non-ideal gases. For more details concerning the model atmospheres used in this work we refer the reader to Rohrmann et al. (2002).

In Fig. 1 we show the emergent spectrum of our $0.280\text{-}M_{\odot}$ He WD model at some selected points of its evolution. The prediction of the present calculations, plotted with solid lines, are compared with our older treatment given in Serenelli et al. (2001). Note that for effective temperatures above ≈ 7000 K, hydrogen lines strongly modify the shape of the flux distribution, so their effect is expected to affect particularly the U and B colours. At low effective temperature, the emergent spectrum is modelled by the CIA opacity, and the bulk of radiation is forced to emerge at higher frequencies as compared with the blackbody prediction. As a result, most colour indices will exhibit a pronounced turn-off to the blue as the effective temperature decreases below ≈ 4000 K. Note finally that the present calculation predicts a flux distribution somewhat different from that of our older treatment. This is due partly to the inclusion of non-ideal effects and also the use of updated CIA opacity data.

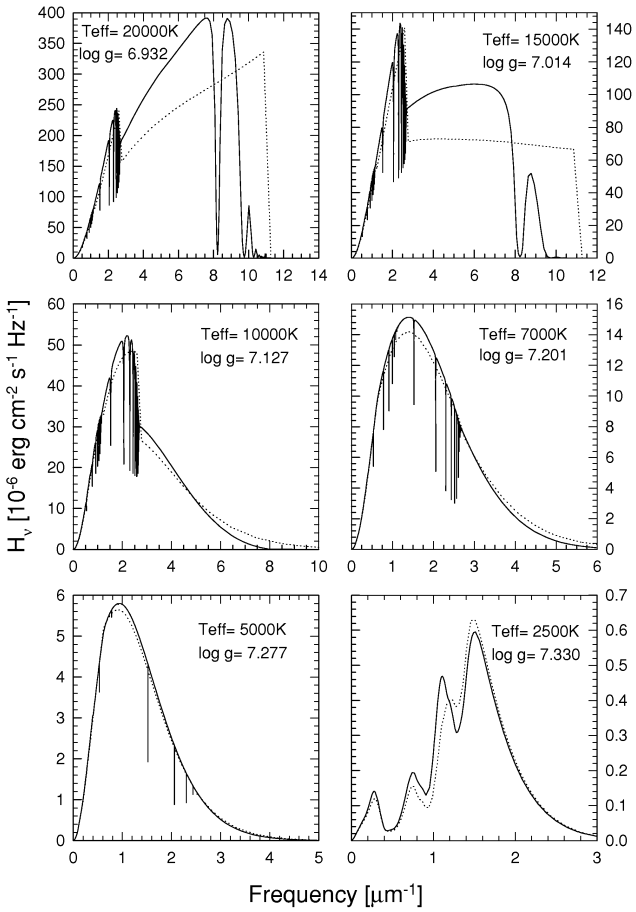

Figure 1. Emergent spectra calculated for some selected models of our evolutionary sequence of 0.280 $M_\odot$ and $Z = 0.0002$. Effective temperatures and surface gravities are indicated in each panel. Models are characterized by pure hydrogen outer layers, resulting from element diffusion. Solid lines show the present calculations including the line opacity, the non-ideal gas model and up-to-date CIA opacities. Dotted lines indicate the results obtained with our previous treatment of model atmospheres.

2.2 Evolutionary code and pre-white dwarf evolution

The evolutionary calculations presented in this work have been carried out with the same evolutionary code as described in Althaus et al. (2001a). Here we briefly present the main physical inputs of the code and refer the reader to that article for a more comprehensive description. WD evolution is accomplished in a self-consistent way with abundance changes as predicted by element diffusion and nuclear burning. In order to achieve this, gravitational settling, and chemical and thermal diffusion of nuclear species have been fully taken into account following the multicomponent gas treatment of Burgers (1969). Hydrogen burning is considered through a complete network of thermonuclear reactions for the proton–proton chain and the CNO bi-cycle. As a result of the various diffusion processes, the metallicity distribution evolves with time; thus radiative opacities are calculated consistently with predictions from element diffusion and are taken from OPAL opacity tables (Iglesias & Rogers 1996).

Initial He WD models have been obtained by abstracting mass from a 1-$M_\odot$ model at appropriate stages of its evolution off the main sequence. We have considered two different metallicity values for our WD progenitor models, $Z = 0.001$ and 0.0002, chosen in order to be representative of low-metallicity environments that are found in many globular clusters. For He WD models more massive than 0.2 $M_\odot$ in the case of a metallicity value $Z = 0.001$ and more massive than 0.23 $M_\odot$ for $Z = 0.0002$, mass loss was invoked at different stages during the evolution along the red giant branch. However, for less massive models we have followed a different procedure. Mass loss is initiated soon after the 1-$M_\odot$ model leaves the main sequence and starts its excursion redwards in the Hertzsprung–Russell diagram (HRD). We have followed the accepted idea that He WDs (particularly low-mass He WDs) are formed in binary systems where the He WD progenitor undergoes a strong mass-loss phase caused by Roche lobe overflow. Indeed, for low-mass models we have computed pre-WD evolution by imposing that mass-loss rates are fixed by the condition that the stellar radius must remain close to the radius of the Roche lobe. To compute the radius of the Roche lobe we assume that our 1-$M_\odot$ model has a 1.4-$M_\odot$ companion (representative of a pulsar companion). Given the initial semi-axis of the orbit, we obtain the radius of the Roche lobe by means of the analytic approximation given by Eggleton (1983):

$$r_{\rm L} = a\frac{0.49q^{2/3}}{0.6q^{2/3} + \ln(1+q^{1/3})}, \tag{1}$$

where $r_{\rm L}$ is the radius of the Roche lobe, a is the semi-axis of the orbit and q is the mass ratio. We have assumed that mass loss from our 1 $M_\odot$ star is fully non-conservative, i.e. all the matter lost from the WD progenitor leaves the system and carries off its intrinsic angular momentum. To this end, we have followed the formulation given by Podsiadlowski, Joss & Hsu (1992), that is

$$\frac{\dot{J}_{\rm ML}}{J} = \frac{M}{M_1 M_2}\dot{M}_1\ {\rm yr}^{-1}. \tag{2}$$

Here, J means the total angular momentum, $\dot{J}_{\rm ML}$ is its time derivative caused by mass loss and M is the total mass of the system. Subscripts 1 and 2 refer to the WD progenitor and the 1.4-$M_\odot$ companion, respectively. Finally, $\dot{M}_1$ is the mass-loss rate of the WD progenitor. In addition, we have also considered angular momentum losses caused by gravitational wave radiation (Landau & Lifshitz 1971)

$$\frac{\dot{J}_{\rm GR}}{J} = -8.5\times10^{-10}\frac{M_1 M_2 M}{a^4}{\rm yr}^{-1}, \tag{3}$$

which is an important contribution to angular momentum losses in binaries with very short periods. Finally, magnetic stellar wind braking when a convective envelope develops has also been accounted for as in Sarna et al. (2000):

$$\frac{\dot{J}_{\rm MB}}{J} = -3\times10^{-7}\frac{M^2 R_1^2}{M_1 M_2 a^5}{\rm yr}^{-1}. \tag{4}$$

In order to follow the time evolution of J, we integrate the equation

$$\frac{\dot{J}}{J} = \frac{\dot{J}_{\rm ML}}{J} + \frac{\dot{J}_{\rm GR}}{J} + \frac{\dot{J}_{\rm MB}}{J} \tag{5}$$

and with the aid of Kepler's third law we finally obtain a (and $r_{\rm L}$ through equation 1). The present treatment for mass loss is not self-consistent since the mass-loss rate is not incorporated as a new unknown quantity to be solved during the iteration procedure in the Henyey scheme used to solve the stellar structure equations, but instead is fixed in advance for each model. However, we want to recall that our main interest in this work is not to analyse the properties (initial/final periods, masses, semi-axis) of binary systems that lead to the formation of He WD millisecond pulsar pairs, but to study the cooling time-scales and photometric properties of cooling He WDs. Also, it is worth mentioning that the algorithm applied in the present work to simulate mass-loss phases represents a much better approach to obtaining physically sound initial He WD models than

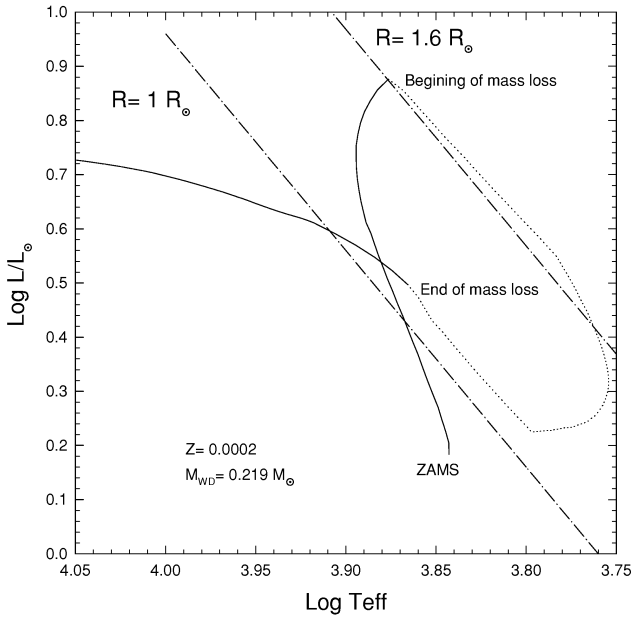

Figure 2 Hertzsprung–Russell diagram for the 0.219-$M_\odot$ WD progenitor with initially 1 $M_\odot$ and $Z = 0.0002$. The dotted line depicts the evolution during the mass-loss phase, which starts when the star fills its Roche lobe at $R = 1.6\,R_\odot$. The initial and final semi-axis are 5.25 and 4.6 $R_\odot$, respectively. The initial and final periods are 0.9 d in both cases.

that of simply abstracting mass as performed previously in Althaus et al. (2001a).

For the purpose of illustration, we show in Fig. 2 the evolution in the HRD for the 0.219-$M_\odot$ WD progenitor having initially 1 $M_\odot$. Note that during the first stages of mass loss, the WD progenitor evolves at almost constant radius. Small deviations from constant-radius evolution are caused by the fact that the semi-axis increases slightly as a result of mass loss from the least massive component of the pair. As evolution proceeds, an outer convection zone develops and magnetic braking starts to play an important role with the consequent result that the orbit starts to shrink. During the final stage of mass loss, the WD progenitor evolves again at constant radius until it eventually shrinks within the Roche lobe and mass loss halts. To place our results on a more quantitative basis we list in Table 1 the main characteristics for some of our less massive WD progenitors. In particular, for a given WD model, we list the metallicity, the surface hydrogen abundance at the end of the mass-loss phase and the initial and final period and semi-axis. We want to mention that our results agree quite well with more detailed calculations in which the mass-loss phase is calculated self-consistently (Sarna et al. 2000).

We want to mention that the assumptions made in our mass-loss treatment give rise to initial He WD models with relatively large hydrogen envelopes, which favours the occurrence of appreciable hydrogen burning and CNO thermonuclear flashes during the WD stage. This is also true if progenitor stars are more massive than the 1-$M_\odot$ value assumed in this work. We have checked this assertion by performing additional calculations on the basis of our mass-loss prescription. However, it is possible that He WDs may also be formed in binary systems that have experienced mass-loss episodes via a common-envelope stage, in which case mass transfer would be unstable. This could be the case for instance if the accretor is a C/O WD (see, for instance, Han 1998). This different evolutionary history for the He WD progenitor could affect the hydrogen layer thickness and accordingly the He WD cooling rate. The treatment of the common envelope stage is a difficult one and it has not been considered in this paper.

Table 1. Main characteristics of some low-mass pre-WD progenitor calculations.

M_f ($M_\odot$)	Z	X_s	P_i (d)	a_i ($R_\odot$)	P_f (d)	a_f ($R_\odot$)
0.199	0.0002	0.390	0.70	4.44	0.36	2.47
0.219	0.0002	0.435	0.90	5.25	0.90	4.60
0.172	0.001	0.357	0.95	5.44	0.26	1.96
0.183	0.001	0.391	1.02	5.71	0.43	2.79
0.197	0.001	0.426	1.05	5.82	0.85	4.40

As stated before, two low-metallicity values have been considered in this study: $Z = 0.001$ and 0.0002 and we have computed a grid of models for each of these values. In the case of $Z = 0.0002$, we have followed the evolution of He WD models with stellar masses of 0.199, 0.209, 0.219, 0.225, 0.243, 0.266, 0.280, 0.300 and 0.319 $M_\odot$; and for the case of $Z = 0.001$ we considered 0.172, 0.183, 0.197, 0.230, 0.244, 0.300, 0.336, 0.380, 0.390, 0.422 and 0.449 $M_\odot$. All of these models were evolved from the end of the mass-loss phase, during the pre-WD evolution, through the stages of hydrogen shell flashes (when they take place) down to very advanced stages of evolution.

3 RESULTS

Qualitatively, the evolution of He WDs with low metallicity is not markedly different from the case of solar metallicity analysed in our previous studies (Althaus et al. 2001a). Indeed, we find that objects with masses above a certain threshold value experience several episodes of hydrogen thermonuclear flashes caused by the massive hydrogen envelopes resulting from binary evolution. The existence of such flash episodes affect the further cooling history of the star. However, the low metal content has an important effect on the evolution of He WDs, particularly regarding the occurrence and characteristics of CNO thermonuclear flashes. In broad outline, CNO flashes become less intense as the metal content is decreased. This is the main reason why loops in the HRD induced by CNO flashes are markedly less extended in the case of lowest metallicity. This is illustrated in Figs 3 and 4, where we present the evolutionary tracks of some selected He WD sequences with an initial metal content $Z = 0.0002$ and 0.001, respectively. It is worth mentioning that the stellar mass threshold ($M_{\rm th}$) for the occurrence of CNO hydrogen flashes depends on the assumed metal content. Specifically, for $Z = 0.001$ and 0.0002 we find a lower-mass limit for the occurrence of CNO flashes of $M_{\rm th} \approx 0.22$ and 0.26 $M_\odot$, respectively (in the case of solar metallicity $M_{\rm th}$ becomes ≈ 0.18 $M_\odot$; see Althaus et al. 2001a). With regard to the upper mass boundary, our most massive model with $Z = 0.0002$ and 0.319 $M_\odot$ is fully unstable, whilst for the case $Z = 0.001$ we find a CNO hydrogen flash even for a stellar mass value as high as 0.422 $M_\odot$, but not in the sequence with $M = 0.449$ $M_\odot$. We also want to comment on the fact that the mass range for the occurrence of hydrogen flashes depends on whether element diffusion is considered or not, as we find previously for the solar metallicity case (Althaus et al. 2001a). For instance, in the absence of diffusion, only our 0.280-, 0.300- and 0.319-$M_\odot$ sequences undergo thermal instabilities in the case of $Z = 0.0002$. For the other metallicity value, $Z = 0.001$, models in the range between approximately 0.24 and 0.35 $M_\odot$, suffer from these instabilities.

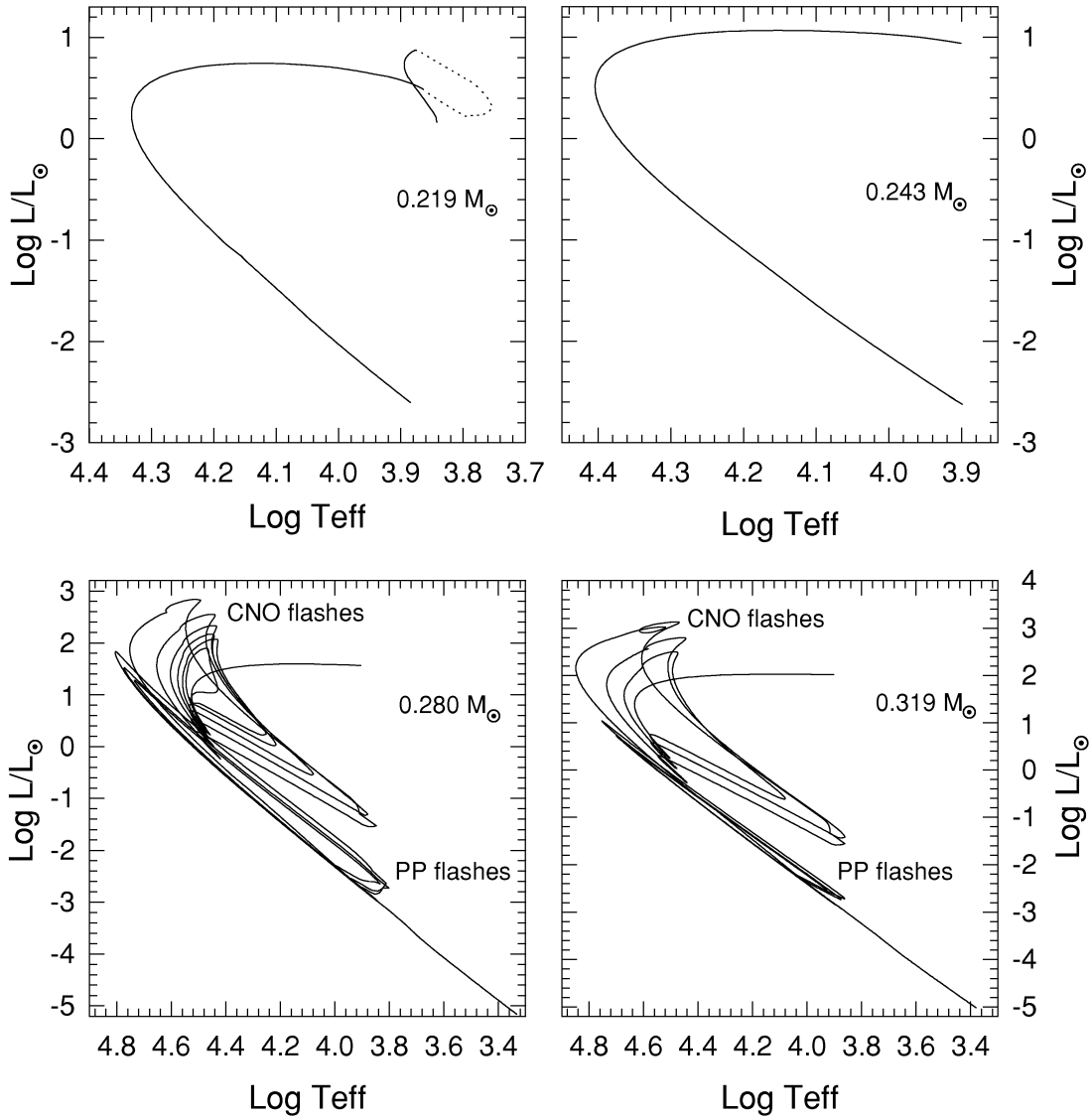

Figure 3. Evolutionary tracks in the Hertzsprung–Russell diagram for some selected masses of our grid for $Z = 0.0002$. Masses of WD models are shown in the plots. For the 0.219-$M_\odot$ model, pre-WD evolution is also shown (as in Fig. 2) and the mass-loss phase is depicted with a dotted line. 0.219- and 0.243-$M_\odot$ models do not suffer from any thermonuclear flashes. However, the 0.280- and 0.319-$M_\odot$ models undergo some hydrogen flashes. Soon after pre-WD evolution these models experience some hydrogen flashes dominated by CNO burning (loops showing moderate redwards excursions in the HRD, labelled CNO flashes in the plots). After these flashes models cool down but when $T_{\rm eff}$ reaches approximately 8000 K another sequence of flashes occur, but in this case completely dominated by hydrogen burning via PP cycle. In the HRD, these models evolve 'up' and 'down' during PP-flashes with almost constant radius (labelled PP flashes in the plots).

A feature worthy of comment predicted by our calculations is the existence of thermal instabilities in models with $Z = 0.0002$ at more advanced stages of evolution than those at which CNO flashes occur. These instabilities are related to unstable hydrogen burning via the proton–proton chains (PP), which dominate hydrogen burning at advanced ages. The existence of such PP flashes can be understood on the basis of a much thicker hydrogen envelope characterizing these models. This is a result of the CNO burning being inefficient in depleting the hydrogen content of the envelope of the star during the pre-WD evolution and during CNO flashes. After the end of CNO flash episodes, the radial extent of the upper boundary of the hydrogen burning shell diminishes as evolution proceeds. At the same time, some hydrogen chemically diffuses downwards to hotter layers. When the burning shell is thin enough, nuclear burning becomes unstable, as predicted by the instability criterion of Kippenhahn & Weigert (1990) (see Driebe et al. 1999 for an application of this instability criterion in the context of CNO flashes in He WDs)

$$C^* = C_P \left(1 - \frac{4\,\nabla_{\rm ad}\delta}{4\alpha - R_{\rm shell}/D} \right) > 0, \qquad (6)$$

where C^* and C_P are the gravothermal and constant pressure specific heats, respectively, $\nabla_{\rm ad}$ is the adiabatic gradient, $\alpha = (\partial \ln \rho/\partial \ln P)_T$, $\delta = -(\partial \ln \rho/\partial \ln T)_P$, $R_{\rm shell}$ is the radial coordinate of the shell and D is its radial extent (defined as the point at which nuclear burning falls below 0.001 of the maximum value). We find that this criterion is fulfilled in our models at the onset of PP flashes at $T_{\rm eff} \approx 8500$ K. In particular, this is because of the large

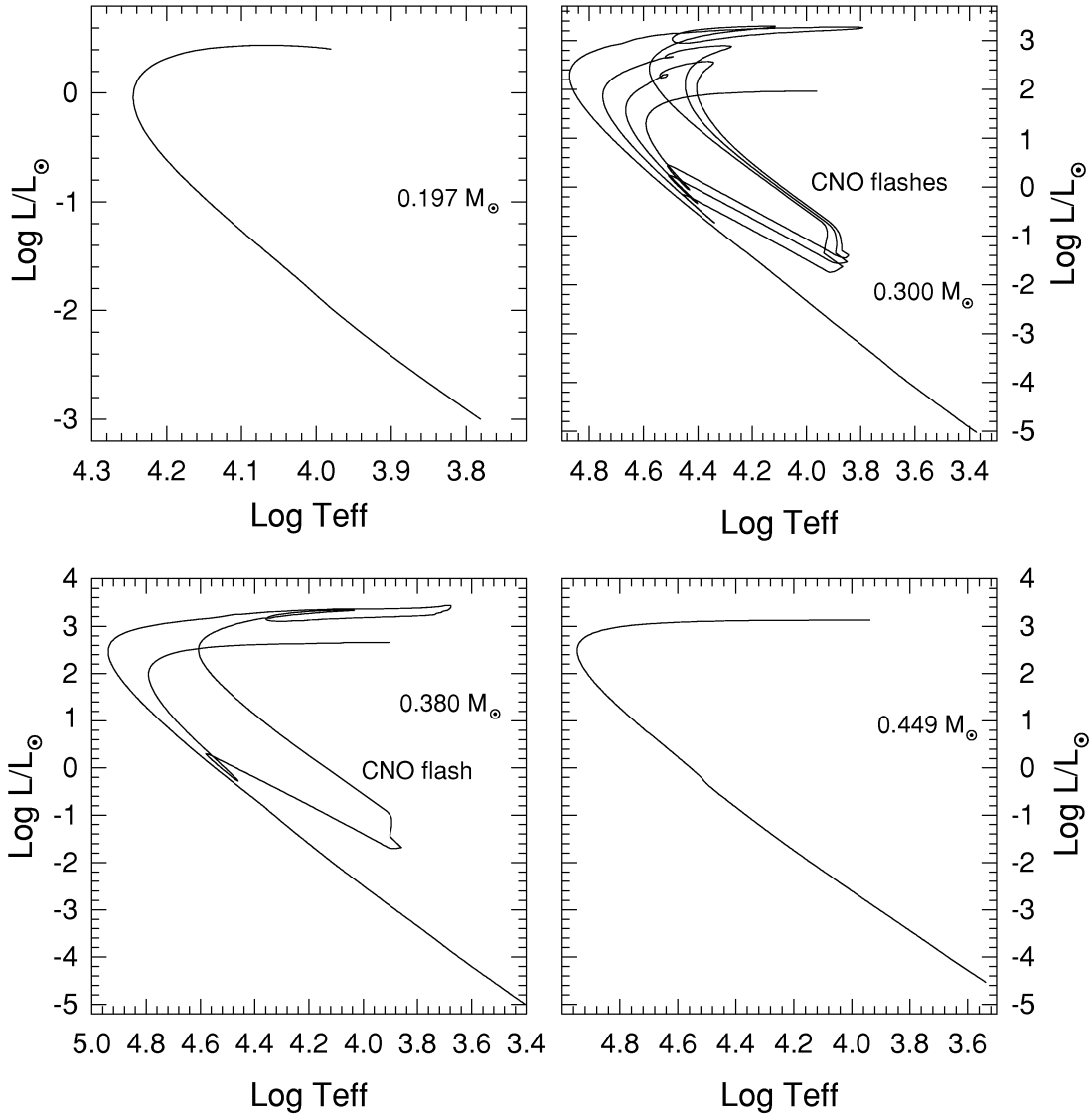

Figure 4. Evolutionary tracks in the Hertzsprung–Russell diagram for some selected models from our grid of $Z = 0.001$ He WDs models. The least massive model does not suffer from any thermonuclear flashes and cools very slowly because of residual nuclear burning, which is a major contribution to the energy budget of the star. At intermediate masses, as represented by our 0.300-$M_{\odot}$ model, element diffusion induces the occurrence of several hydrogen flashes dominated by CNO burning. For higher masses the number of CNO flashes diminishes (0.380 $M_{\odot}$) and finally for the highest-mass value we find that no flash occurs at all (0.449 $M_{\odot}$).

values reached by the quantity $R_{\rm shell}/D$, which exceeds 10 at the onset of the flash; while α and δ are close to 0.85 and 0.60, respectively.

PP-induced flashes differ from their CNO counterparts in some respects. For instance, in most cases PP flashes are less intense than the CNO ones and during flash episodes convective mixing in the outer layers of the star is less frequent than for CNO flashes. An interesting characteristic of these flashes is that after a PP hydrogen flash is initiated, the star is forced to move in the HR diagram following lines of almost constant radii close to the cooling track. Also, during each of these PP flashes, the total amount of hydrogen in the star is barely reduced by nuclear burning with the result that the star in general will experience numerous episodes of this kind. In the sequences with $Z = 0.001$ only those models that lack CNO flashes experience PP hydrogen flashes, but they occur at extremely high ages. All of our sequences with $Z = 0.0002$ are characterized by PP hydrogen flashes even if they have experienced CNO flashes earlier in their evolution. The important point to emphasize here is that the PP flashes are induced by chemical diffusion that carries some hydrogen downwards deep enough for the star to ignite hydrogen there. Except for the less massive models ($M \lesssim 0.25$ $M_{\odot}$), PP flashes in the sequences with $Z = 0.0002$ take place between 2 and 4 Gyr after the end of mass-loss episodes. In general, the more massive the He WD, the earlier in the life of the star these PP flashes occur. It is worth emphasizing again that the existence of such PP flashes in He WDs is restricted to the case of metallicity much lower than the solar metallicity. For instance, such flashes are absent in the case of models with $Z = 0.02$, and only our 0.172- and 0.183-$M_{\odot}$ models with $Z = 0.001$ suffer from them. The fact that essentially models with extremely low metal content experience PP flashes can be understood on the basis that such models are left with hydrogen envelopes so massive that the tail of the hydrogen

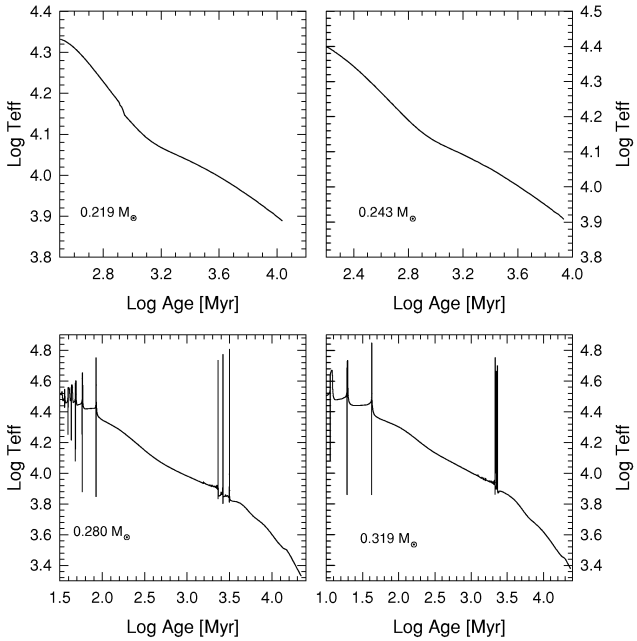

Figure 5. The effective temperature as a function of age for the same models as shown in Fig. 3 ($Z = 0.0002$). For more massive models, spikes correspond to evolutionary stages during flash episodes. It is clear that models that experience unstable burning reach very low effective temperatures well within 15 Gyr.

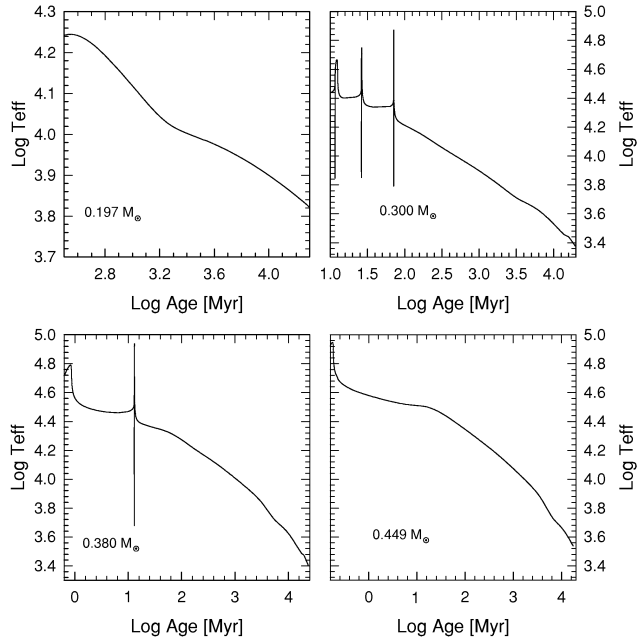

Figure 6. The effective temperature as a function of age for the same models as shown in Fig. 4 ($Z = 0.001$). Spikes correspond to evolutionary stages during flash episodes. As shown in Fig. 5, models characterized by unstable burning reach very low effective temperatures well within 15 Gyr. For the 0.449-$M_\odot$ sequence a short evolutionary time-scale is obtained even in the absence of thermonuclear flashes.

distribution chemically diffusing inwards reaches hot enough layers. This increases the hydrogen burning by PP reactions and leads to a thermal instability.

In Figs 5 and 6 we show the effective temperature as a function of cooling age for the same stellar mass values as given in Figs 3 and 4, respectively. Note that the lack of CNO thermonuclear flashes in less massive models leads to a very slow rate of evolution, i.e. such models remain relatively bright even at very large ages. This is so because stable hydrogen shell burning via PP nuclear reactions constitutes the main source of luminosity over most of the entire evolution of these models. In contrast, the existence of diffusion-induced CNO thermonuclear flashes leads eventually to He WD models with hydrogen envelope masses small enough for nuclear burning to not appreciably contribute to the luminosity budget of the star. Accordingly, such models are characterized by short evolutionary time-scales. This age dichotomy between models with and without CNO flashes also manifests itself in cooling sequences with a solar metal content (Althaus et al. 2001a). It is worth noting that such a dichotomy is less accentuated in the case of models with very low metal content. To place this assertion on a more quantitative basis, we mention that in reaching a value of $T_{\rm eff} = 8000$ K, models with 0.219, 0.243, 0.280 and 0.319 $M_\odot$ ($Z = 0.0002$) need approximately 10, 8.7, 3.1 and 2.3 Gyr, respectively. In the case of $Z = 0.001$, models with 0.197, 0.300, 0.380 and 0.449 $M_\odot$ need approximately 10, 1, 2.2 and 3.1 Gyr, respectively. The dependence of the cooling history on the assumed initial metallicity can be understood by inspecting Fig. 7 in which we show the time dependence of hydrogen burning luminosity for our 0.300-$M_\odot$ sequences with $Z = 0.001$ and 0.0002. In the case of $Z = 0.001$, after 1.5 Gyr of the occurrence of CNO flashes, stable hydrogen burning reaches a maximum contribution to surface luminosity of 35 per cent. Afterwards, nuclear burning becomes less important as evolution proceeds. For instance, at 4 Gyr, it only contributes less than 10 per cent to the

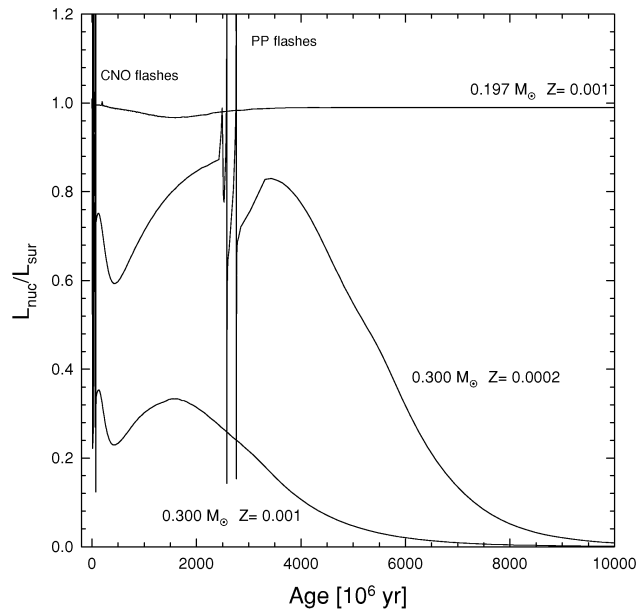

Figure 7. Hydrogen burning luminosity in terms of surface luminosity as a function of age for our 0.197 ($Z = 0.001$) and 0.300 ($Z = 0.001$ and 0.0002) He WD models. Note that for the lowest mass shown, the lack of thermonuclear flashes causes surface luminosity to be almost exclusively supported by stable hydrogen burning. In contrast, for more massive models, stable nuclear burning following the flash episodes contributes only partially to the energy budget of the star. Note also that as Z is increased, the contribution of residual hydrogen burning becomes less important.

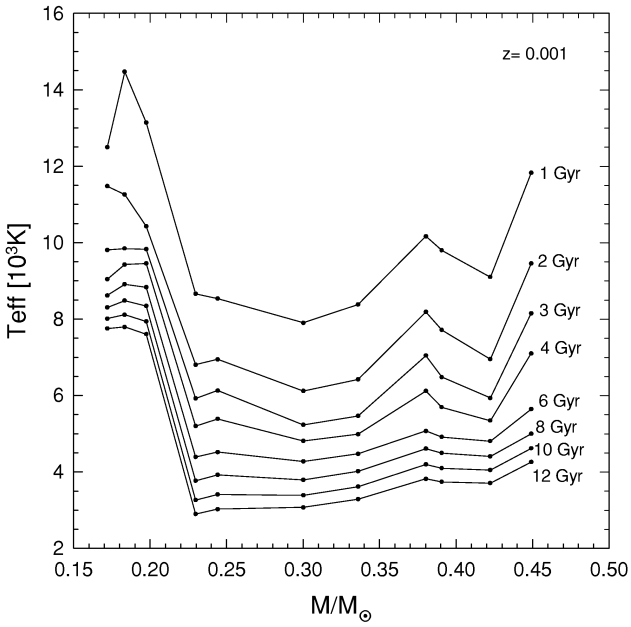

Figure 8. Isochrones for our He WD sequences with $Z = 0.001$. The abrupt drop shown by isochrones in the range 0.20–0.22 $M_\odot$ is a consequence of the existence of a mass threshold for the occurrence of CNO flashes. Much shorter cooling ages result if the mass of the model is above this threshold value. The bump exhibited by the isochrones at ≈ 0.38 $M_\odot$ is related to an increase in the efficiency of PP stable nuclear burning at low ages. For further details see the text.

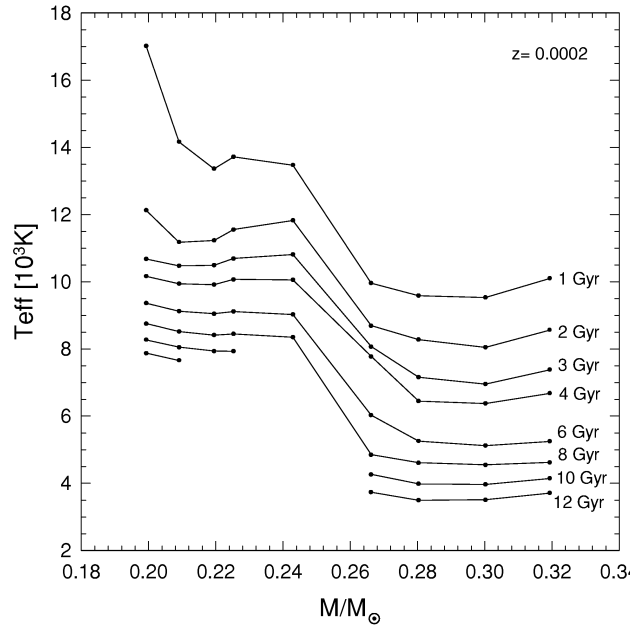

Figure 9. Same as in Fig. 9 but for the case $Z = 0.0002$. Here isochrones exhibit a not so pronounced drop as in the case of $Z = 0.001$ models. For models that not suffer from CNO flashes, calculations were stopped before PP flashes begin and thus, some low-mass models have not reached ages as large as 10 Gyr (for this reason, the 10- and 12-Gyr isochrones do not join up).

luminosity of the star. In contrast, in the case of $Z = 0.0002$, stable nuclear burning contributes appreciably to surface luminosity even at an age of 6 Gyr. After CNO flashes, stable nuclear burning contributes more than 60 per cent of the energy radiated by the star within the first 5 Gyr. This contribution drops rather abruptly during the subsequent stages of evolution, eventually reaching 10 per cent at 7 Gyr. With regard to Fig. 7, let us finally mention that we have also included the 0.197-$M_\odot$ sequence ($Z = 0.001$), which does not suffer from flash episodes. In this case, the stellar luminosity is completely supported by stable hydrogen burning along the entire cooling branch, which is clearly shown in Fig. 7.

In Figs 8 and 9 we plot the isochrones for some selected ages in the mass-effective temperature plane for our $Z = 0.001$ and 0.0002 models, respectively. Note that at the stellar mass threshold, $M_{\rm th}$, the isochrone plots exhibit a pronounced discontinuity. This is not surprising in view of the age dichotomy discussed earlier. The plot corresponding to $Z = 0.001$ models resembles that of He WD models with an initial solar-like metal content (Althaus, Serenelli & Benvenuto 2001b). This is particularly true regarding the presence of an age dichotomy at, in this case, $M_{\rm th} \sim 0.22$ $M_\odot$. We judge that future observations of low-mass WDs with millisecond pulsar companions formed in low-metallicity environments could eventually place our predictions on solid observational grounds.[1] Another feature worthy of comment depicted by Fig. 8 is the existence of a bump in the isochrone curves at 0.380–0.390 $M_\odot$, particularly at low ages. This behaviour can be understood on the basis of the role played by stable PP hydrogen burning after CNO flash episodes. Specifically, after experiencing only one CNO flash, the 0.380- and 0.390-$M_\odot$ models are left with a hydrogen envelope thin enough so as to inhibit the occurrence of another CNO flash. However, envelopes are thick enough to maintain an appreciable amount of nuclear energy release through stable PP hydrogen burning, thus slowing the cooling rate at intermediate stages of evolution. Finally, note the increasing isochrone curves for the most massive sequence, which does not undergo any thermonuclear flash, thus resulting in comparatively large cooling ages. The situation for the case of $Z = 0.0002$ sequences is qualitatively similar, though the age dichotomy is less noticeable and it is located at $M_{\rm th} \sim 0.25$–0.26 $M_\odot$. As explained earlier, this is a result of the fact that, in this case, during flash episodes CNO cycle reactions are less efficient than for higher metallicities and thus, the hydrogen envelope is not so drastically consumed.

The evolution of our He WD models in the colour–magnitude diagrams is illustrated in Fig. 10, which shows the run of the absolute visual magnitude M_V for our models as a function of the colour indices $U - V$ and $V - I$. Note that models that have suffered from CNO thermonuclear flashes show a turn-off in the $V - I$ colour at $M_V \approx 16$ and $V - I \approx 1.4$. This turn-off, which results from the strong CIA opacity by molecular hydrogen at low temperatures, is reached well within 15 Gyr, mostly by He WDs with $Z = 0.001$. After reaching the turn-off, the emergent spectrum becomes bluer and remains brighter than $M_V \approx 17$ with subsequent cooling. A similar trend has also been found for the case of solar metallicity (Serenelli et al. 2001), though in that situation He WDs with stellar masses even as low as ≈ 0.19 $M_\odot$ reach high magnitude values.

In Fig. 10 we have also included the recent observational data of Taylor et al. (2001) and Edmonds et al. (2001) for the He WD candidates in the globular clusters NGC 6397 and 47 Tucanae, respectively. For NGC 6397 we have adopted a distance modulus $(m - M)_V = 12.29$ and $E(B - V) = 0.18$ (Cool et al. 1998). In the case of 47 Tucanae, $(m - M)_V = 13.39$ and $E(B - V) = 0.055$ (Zoccali et al. 2001) were used to transform to absolute magnitudes

[1] Tentative support for the existence of such an age dichotomy is given by the field He WD companions to PSR B1855+09 and PSR J1012+5307 ms pulsars (Althaus et al. 2001a,b).

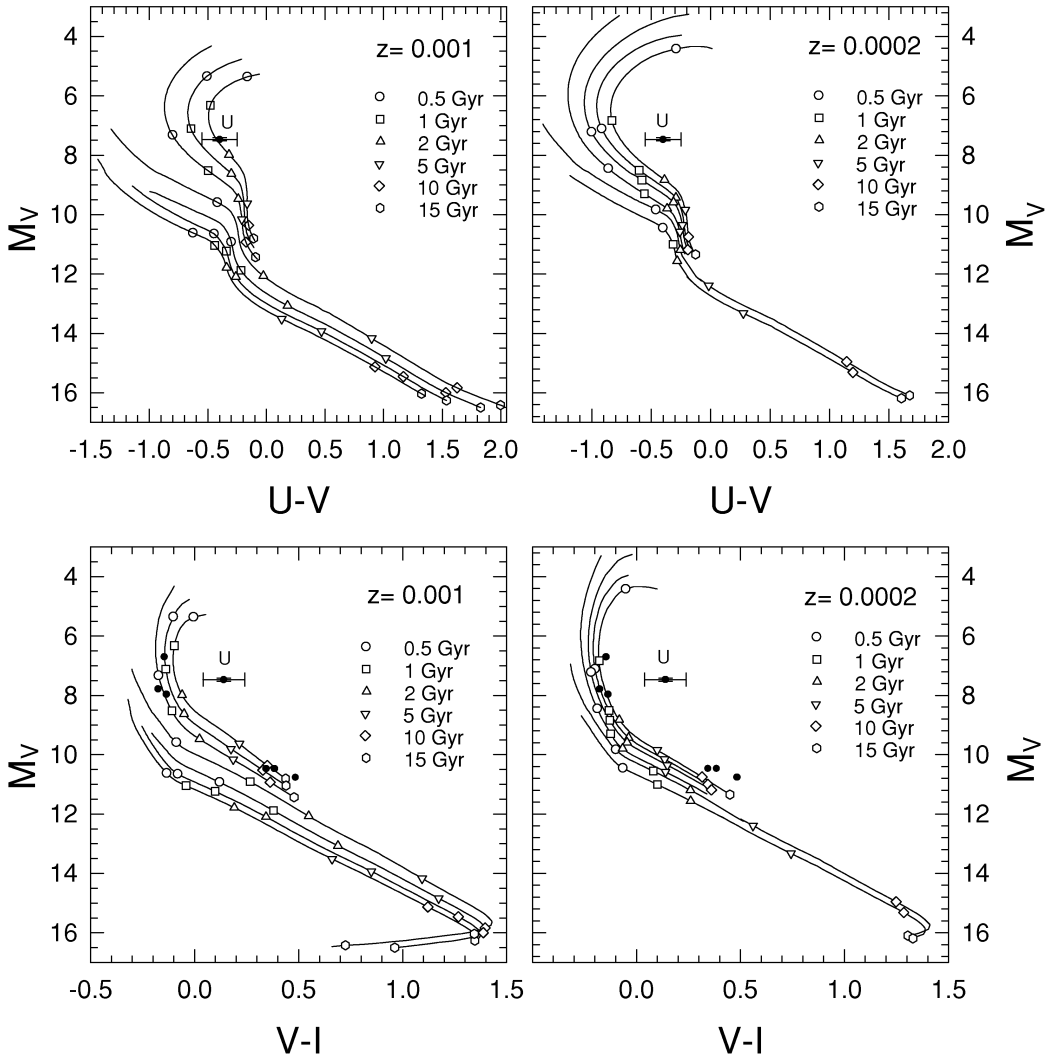

Figure 10. The absolute visual magnitude in terms of the colour indices $U-V$ (upper panels) and $V-I$ (bottom panels) for He WD models with stellar masses (from right to left) 0.172, 0.183, 0.197, 0.230, 0.300, 0.380 and 0.449 $M_\odot$ for $Z=0.001$, and 0.199, 0.209, 0.219, 0.243, 0.266 and 0.319 $M_\odot$ for $Z=0.0002$. Symbols along the curves denote some selected ages. In addition, the observational data for the He WD in 47 Tucanae (Edmonds et al. 2001; denoted by 'U') and the six He WD candidates in NGC 6397 reported by Taylor et al. (2001, filled circles) are included in the figure.

and to deredden colour indices. In both cases, extinction laws from Holtzman et al. (1995) were applied. Let us consider first the He WD candidates in NGC 6397. Given the metal content for NGC 6397 ([Fe/H $=-1.82$]; Anthony-Twarog & Twarog 2000), then our $Z=0.0002$ sequences are appropriate for a direct comparison with observations. Note that the six He WD candidates in NGC 6397 can be split into two groups. In particular, for the three brightest stars of the observed sequence, our evolutionary models fit the observational data quite well. We find that such He WDs would be characterized by stellar mass values in the range 0.2–0.22 $M_\odot$, which is below the mass value for the occurrence of CNO flashes. With regard to age determination, we find ages between 0.5 and 1.5 Gyr for these stars. In contrast, the three dimmest stars appear to have larger radii even compared with our least massive model ($\approx$ 0.2 $M_\odot$), as is clear from the lower right-hand panel of Fig. 10. We want to point out that, based on our mass-loss treatment, we find a minimum mass value for the resulting He core remnant that is very close to 0.2 $M_\odot$ for progenitors with $Z=0.0002$. We have checked this by performing additional pre-WD calculations for different initial binary configurations. In this context, Burderi, D'Antona & Burgay (2002) have also found that their evolutionary models have smaller radii than those required to fit the observational data. In addition, they also find a minimum mass limit of $\approx$ 0.2 $M_\odot$ for He WDs with very low-metallicity progenitors. However, it is worth noting that our models are somewhat less compact than those presented by Burderi et al. (2002). We judge that this difference could be a result of the fact that in our calculations we have included chemical element diffusion that leads to pure hydrogen envelopes and thus to models with larger radii (Althaus et al. 2001a), thus reducing the discrepancy with observations. Another point worthy of comment in connection with this second group of He WD candidates is related to their ages. Indeed, our least massive sequence yields cooling ages between 10 and 15 Gyr for these stars.[2] If we take into account the time elapsed during the pre-WD evolution (which is approximately

[2] We stress again that such large ages are expected because our less massive models are characterized by mass values well below the $M_{\rm th}$ value for the occurrence of CNO thermonuclear flashes.

Table 2. Selected stages for 0.199-, 0.243- and 0.30-$M_\odot$ He WD models for metallicity $Z = 0.0002$.

$M_*/M_\odot$	$T_{\rm eff}$	Log (g)	Age (Gyr)	$U-B$	$B-V$	$V-R$	$V-K$	$R-I$	$J-H$	$H-K$	BC	M_V
0.199	8 920	4.3218	0.295	−0.09	0.10	0.04	0.12	0.06	0.07	−0.09	−0.09	4.41
”	10 780	4.5281	0.494	−0.24	−0.05	−0.03	−0.20	−0.02	0.02	−0.10	−0.40	4.42
”	14 220	5.0085	0.683	−0.52	−0.13	−0.07	−0.45	−0.07	−0.02	−0.12	−1.08	5.09
”	16 150	5.3500	0.791	−0.64	−0.15	−0.08	−0.54	−0.09	−0.04	−0.13	−1.41	5.72
”	16 880	5.5465	0.861	−0.68	−0.16	−0.08	−0.57	−0.10	−0.04	−0.13	−1.52	6.14
”	17 110	5.6901	0.924	−0.69	−0.15	−0.08	−0.58	−0.10	−0.04	−0.13	−1.56	6.47
”	16 810	5.9008	1.054	−0.68	−0.14	−0.08	−0.56	−0.10	−0.04	−0.13	−1.51	7.03
”	16 430	5.9817	1.124	−0.66	−0.13	−0.08	−0.55	−0.09	−0.04	−0.13	−1.45	7.27
”	15 960	6.0522	1.201	−0.64	−0.12	−0.08	−0.53	−0.09	−0.03	−0.13	−1.37	7.49
”	15 430	6.1141	1.283	−0.61	−0.11	−0.07	−0.50	−0.08	−0.03	−0.12	−1.28	7.71
”	14 870	6.1704	1.375	−0.58	−0.09	−0.07	−0.47	−0.08	−0.02	−0.12	−1.19	7.91
”	14 280	6.2219	1.478	−0.54	−0.08	−0.07	−0.45	−0.07	−0.02	−0.12	−1.08	8.11
”	13 700	6.2699	1.594	−0.51	−0.06	−0.06	−0.41	−0.06	−0.01	−0.12	−0.97	8.30
”	13 110	6.3151	1.725	−0.47	−0.04	−0.06	−0.38	−0.06	−0.01	−0.12	−0.86	8.49
”	12 530	6.3582	1.876	−0.43	−0.01	−0.05	−0.34	−0.05	0.00	−0.12	−0.74	8.68
”	11 960	6.4003	2.058	−0.39	0.02	−0.04	−0.29	−0.04	0.01	−0.11	−0.63	8.88
”	11 430	6.4419	2.295	−0.36	0.05	−0.03	−0.24	−0.02	0.02	−0.11	−0.53	9.07
”	10 930	6.4858	2.669	−0.35	0.08	−0.02	−0.18	−0.01	0.03	−0.11	−0.43	9.28
”	10 470	6.5314	3.356	−0.35	0.11	0.00	−0.12	0.01	0.03	−0.11	−0.34	9.49
”	9 990	6.5726	4.351	−0.37	0.15	0.03	−0.04	0.04	0.05	−0.10	−0.26	9.72
”	9 510	6.6103	5.577	−0.39	0.18	0.06	0.08	0.07	0.06	−0.10	−0.21	9.98
”	9 040	6.6448	6.985	−0.42	0.22	0.10	0.21	0.10	0.08	−0.09	−0.17	10.24
”	8 570	6.6772	8.658	−0.45	0.26	0.13	0.34	0.13	0.10	−0.08	−0.14	10.53
”	8 110	6.7069	10.622	−0.47	0.29	0.17	0.49	0.17	0.13	−0.07	−0.13	10.82
”	7 250	6.7575	15.738	−0.48	0.36	0.23	0.81	0.23	0.18	−0.04	−0.11	11.42
0.243	15 050	4.4210	0.131	−0.59	−0.18	−0.08	−0.51	−0.09	−0.03	−0.12	−1.21	3.29
”	21 020	5.0959	0.161	−0.84	−0.23	−0.10	−0.72	−0.13	−0.07	−0.14	−2.10	4.42
”	23 930	5.4719	0.178	−0.93	−0.24	−0.11	−0.80	−0.14	−0.08	−0.15	−2.44	5.13
”	25 070	5.7041	0.190	−0.95	−0.24	−0.12	−0.82	−0.15	−0.08	−0.15	−2.56	5.63
”	25 360	5.8768	0.201	−0.96	−0.24	−0.12	−0.83	−0.15	−0.09	−0.16	−2.59	6.04
”	24 650	6.1290	0.229	−0.94	−0.23	−0.12	−0.81	−0.14	−0.08	−0.15	−2.51	6.72
”	23 920	6.2282	0.250	−0.93	−0.22	−0.11	−0.79	−0.14	−0.08	−0.15	−2.43	7.02
”	23 020	6.3141	0.277	−0.91	−0.21	−0.11	−0.77	−0.14	−0.07	−0.15	−2.33	7.30
”	22 000	6.3880	0.310	−0.88	−0.19	−0.10	−0.74	−0.13	−0.07	−0.15	−2.21	7.56
”	20 900	6.4526	0.350	−0.85	−0.18	−0.10	−0.71	−0.12	−0.06	−0.14	−2.08	7.81
”	19 780	6.5089	0.396	−0.81	−0.16	−0.10	−0.67	−0.12	−0.06	−0.14	−1.93	8.05
”	18 650	6.5594	0.451	−0.77	−0.14	−0.09	−0.64	−0.11	−0.05	−0.14	−1.78	8.27
”	17 540	6.6058	0.517	−0.72	−0.12	−0.09	−0.59	−0.10	−0.04	−0.13	−1.61	8.49
”	16 460	6.6489	0.596	−0.68	−0.10	−0.08	−0.55	−0.09	−0.04	−0.13	−1.44	8.71
”	15 420	6.6900	0.695	−0.63	−0.08	−0.07	−0.51	−0.08	−0.03	−0.13	−1.27	8.92
”	14 450	6.7296	0.826	−0.57	−0.05	−0.07	−0.46	−0.07	−0.02	−0.12	−1.10	9.13
”	13 540	6.7702	1.031	−0.52	−0.02	−0.06	−0.41	−0.06	−0.01	−0.12	−0.93	9.34
”	12 700	6.8121	1.418	−0.46	0.01	−0.05	−0.35	−0.05	0.00	−0.12	−0.77	9.57
”	11 870	6.8494	1.999	−0.42	0.05	−0.04	−0.28	−0.03	0.01	−0.11	−0.61	9.79
”	11 060	6.8826	2.771	−0.41	0.09	−0.01	−0.20	0.00	0.03	−0.11	−0.45	10.02
”	10 290	6.9114	3.712	−0.42	0.14	0.02	−0.08	0.03	0.04	−0.11	−0.31	10.27
”	9 560	6.9384	4.897	−0.44	0.18	0.07	0.09	0.07	0.06	−0.10	−0.23	10.58
”	8 240	6.9865	8.308	−0.49	0.26	0.16	0.46	0.16	0.12	−0.07	−0.14	11.25
0.300	24 990	6.9774	0.065	−0.97	−0.21	−0.12	−0.82	−0.15	−0.08	−0.16	−2.53	8.57
”	23 390	6.9941	0.067	−0.93	−0.19	−0.11	−0.78	−0.14	−0.07	−0.15	−2.36	8.73
”	21 800	7.0043	0.076	−0.89	−0.17	−0.10	−0.74	−0.13	−0.07	−0.15	−2.18	8.88
”	20 050	7.0178	0.105	−0.83	−0.15	−0.10	−0.68	−0.12	−0.06	−0.14	−1.96	9.06
”	18 730	7.0331	0.133	−0.79	−0.13	−0.09	−0.64	−0.11	−0.05	−0.14	−1.78	9.21
”	17 510	7.0495	0.162	−0.74	−0.10	−0.09	−0.60	−0.10	−0.04	−0.13	−1.60	9.36
”	16 160	7.0699	0.199	−0.68	−0.08	−0.08	−0.54	−0.09	−0.03	−0.13	−1.39	9.55
”	14 930	7.0903	0.241	−0.62	−0.05	−0.07	−0.48	−0.07	−0.02	−0.12	−1.18	9.73
”	13 770	7.1113	0.293	−0.55	−0.01	−0.06	−0.42	−0.06	−0.01	−0.12	−0.97	9.93
”	12 870	7.1293	0.350	−0.50	0.03	−0.05	−0.36	−0.05	0.00	−0.12	−0.80	10.10
”	12 050	7.1470	0.424	−0.46	0.06	−0.04	−0.29	−0.03	0.01	−0.12	−0.64	10.27
”	11 110	7.1691	0.558	−0.45	0.10	−0.01	−0.20	0.00	0.02	−0.11	−0.45	10.48
”	10 270	7.1897	0.749	−0.46	0.15	0.03	−0.06	0.04	0.04	−0.11	−0.32	10.75
”	9 470	7.2094	1.024	−0.48	0.19	0.08	0.12	0.08	0.07	−0.09	−0.23	11.06
”	8 870	7.2239	1.336	−0.50	0.22	0.12	0.28	0.12	0.09	−0.08	−0.19	11.34

Table 2 – *continued*

$M_*/M_\odot$	$T_{\rm eff}$	Log (g)	Age (Gyr)	$U-B$	$B-V$	$V-R$	$V-K$	$R-I$	$J-H$	$H-K$	BC	M_V
A”	8 290	7.2368	1.766	−0.51	0.26	0.16	0.46	0.16	0.12	−0.07	−0.15	11.63
B”	7 800	7.2634	2.776	−0.51	0.30	0.19	0.61	0.20	0.15	−0.06	−0.13	11.94
”	7 150	7.2688	2.796	−0.48	0.37	0.24	0.85	0.25	0.19	−0.03	−0.12	12.32
”	6 570	7.2731	3.751	−0.42	0.44	0.29	1.09	0.30	0.23	−0.01	−0.11	12.69
”	6 060	7.2852	4.394	−0.33	0.53	0.35	1.33	0.35	0.27	0.01	−0.12	13.08
”	5 210	7.3257	5.748	−0.11	0.72	0.47	1.82	0.47	0.32	0.07	−0.21	13.93
”	4 840	7.3486	6.969	0.00	0.82	0.53	2.07	0.53	0.35	0.09	−0.31	14.40
”	4 470	7.3622	8.269	0.12	0.92	0.59	2.23	0.59	0.33	0.04	−0.42	14.89
”	4 110	7.3696	9.479	0.22	1.01	0.65	2.12	0.65	0.12	−0.02	−0.46	15.32
”	3 770	7.3743	10.729	0.29	1.07	0.69	1.67	0.68	−0.14	−0.14	−0.41	15.65
”	3 460	7.3785	12.260	0.36	1.13	0.72	1.12	0.68	−0.30	−0.28	−0.31	15.93
”	3 180	7.3835	15.016	0.44	1.19	0.72	0.59	0.60	−0.37	−0.36	−0.16	16.16
”	2 920	7.3858	16.606	0.51	1.24	0.69	0.05	0.43	−0.38	−0.47	0.01	16.37

Ages are counted from the end of mass transfer. Letters A and B denote the age interval during which the 0.30-$M_\odot$ model return several times to high-$T_{\rm eff}$ values as a result from PP hydrogen flashes.

6–7 Gyr for a 1-$M_\odot$ progenitor), then the age of these stars would be in the range 16–21 Gyr, larger than the age of the cluster, which is 12 ± 0.8 Gyr (Anthony-Twarog & Twarog 2000). This suggests that the progenitors of these He WD candidates should have been more massive than 1 $M_\odot$ with, therefore, shorter pre-WD evolutionary ages. To explore this possibility, we have performed additional calculations with our mass-loss prescription. For instance, we found that starting from a 1.4-$M_\odot$ progenitor with a 1.4-$M_\odot$ companion and an initial period of 0.5 d, the pre-WD evolution lasts for approximately 3 Gyr and the mass of the WD remnant is 0.195 $M_\odot$. This would help to alleviate the age discrepancy mentioned above. In this regard, we believe that a more comprehensive exploration of the binary nature leading to the formation of He WDs, particularly for progenitors with very low metal content, is worth carrying out.

With regard to the He WD candidate in the globular cluster 47 Tucanae, we find that our evolutionary models with $Z = 0.001$, a metallicity value not very different from that of 47 Tucanae ([Fe/H = −0.76]), yield a good agreement with observations for the $U-V$ index. In particular, we derive a stellar mass value of ≈ 0.17 $M_\odot$ and a cooling age of approximately 1.5 Gyr for the WD. This age is consistent with the 2 Gyr value corresponding to the spin-down age of the millisecond pulsar companion to the WD (Edmonds et al. 2001 and references cited therein). Note that, as far as the $V-I$ index is concerned, we find no agreement with observational data. In fact, our evolutionary models are located too far to the blue. A lower stellar mass value ($M \approx 0.15$–0.16 $M_\odot$) than our lowest-mass sequence would be needed to match the observed $V-I$. In the case of $Z = 0.0002$ and for the stellar masses we considered, we find no agreement with observations for neither of the metallicities.

Finally, we list in Tables 2 and 3 some colour indices for He WD models with, respectively, $Z = 0.0002$ and 0.001 at selected effective temperature values. We also list the surface gravity (g), the age (in Gyr), the bolometric correction (BC) and the absolute visual magnitude (M_V).

4 CONCLUSIONS

In this study we have explored the evolution of helium-core white dwarf stars with progenitors having much lower metallicities than the solar metallicity usually assumed in the modelling of these stars. The models presented here are appropriate for the interpretation of recent and future observations of low-mass WDs in globular clusters. Specifically, two low-metallicity values have been considered: $Z = 0.001$ and 0.0002. In the case of $Z = 0.0002$, we have followed the evolution of He WD models with stellar masses of 0.199, 0.209, 0.219, 0.225, 0.243, 0.266, 0.280, 0.300 and 0.319 $M_\odot$; and for the case of $Z = 0.001$ we considered 0.172, 0.183, 0.197, 0.230, 0.244, 0.300, 0.336, 0.380, 0.390, 0.422 and 0.449 $M_\odot$. All of these models were evolved from the end of the mass-loss phase down to very advanced phases of evolution. The binary nature of our He WD models has been simulated by abstracting mass from a 1-$M_\odot$ model at appropriate stages of its evolution off the main sequence. Specifically, to obtain physically sound initial low-mass He WD models, mass transfer rates were derived by imposing that the stellar radius remains close to the radius of the Roche lobe. A fully non-conservative approach was assumed and the loss of angular momentum caused by gravitational wave emission and magnetic stellar wind braking have been taken into account.

The evolution of our He WD models has been computed in a self-consistent way with the predictions of time-dependent element diffusion and nuclear burning. A non-grey treatment for the atmosphere that considered the energy transfer by radiation and convection has been employed to derive the outer boundary conditions of our evolving models. Model atmospheres are based on a detailed treatment of the microphysics entering the WD atmospheres, such as non-ideal effects in the equation of state (as given by the occupation formalism of Hummer & Mihalas 1988) and the inclusion of the hydrogen line (from the Balmer, Lyman and Paschen series) and pseudo-continuum opacities. Also, up-to-date collision-induced absorption data (Rohrmann et al. 2002) were incorporated in the computations. Such a detailed description allowed us to provide a grid of accurate colour indices and magnitudes at both early and advanced evolutionary stages, significantly improving previous efforts (Serenelli et al. 2001).

A feature worthy of comment predicted by our calculations is the existence of thermonuclear flash episodes for most of our He WD sequences. In part, this is a result of including in our computations the various chemical diffusion processes. We find that the lower the metallicity Z, the larger the minimum stellar mass for the occurrence of hydrogen thermonuclear flashes induced by the CNO cycle reactions. Specifically, for $Z = 0.001$ and 0.0002 we find a lower-mass limit for the existence of CNO flashes of $M \approx 0.22$ and 0.26 $M_\odot$, respectively (in the case of $Z = 0.02$ such a limit

Table 3. Selected stages for 0.172-, 0.230-, 0.336- and 0.449-$M_\odot$ He WD models for metallicity $Z = 0.001$.

$M_*/M_\odot$	$T_{\rm eff}$	Log (g)	Age (Gyr)	$U-B$	$B-V$	$V-R$	$V-K$	$R-I$	$J-H$	$H-K$	BC	M_V
0.172	9 390	4.6630	0.349	−0.13	0.07	0.02	0.02	0.03	0.05	−0.09	−0.16	5.27
”	12 420	5.2994	0.973	−0.40	−0.07	−0.05	−0.33	−0.05	0.00	−0.11	−0.74	6.22
”	12 760	5.4971	1.173	−0.42	−0.07	−0.05	−0.35	−0.05	0.00	−0.11	−0.81	6.67
”	12 700	5.6392	1.356	−0.42	−0.06	−0.05	−0.35	−0.05	0.00	−0.11	−0.79	7.03
”	12 410	5.7509	1.544	−0.40	−0.05	−0.05	−0.33	−0.05	0.00	−0.11	−0.73	7.35
”	12 010	5.8440	1.746	−0.37	−0.03	−0.04	−0.30	−0.04	0.01	−0.11	−0.65	7.64
”	11 540	5.9253	1.971	−0.33	0.00	−0.04	−0.26	−0.03	0.01	−0.11	−0.56	7.93
”	11 040	5.9987	2.223	−0.30	0.04	−0.03	−0.20	−0.02	0.02	−0.11	−0.46	8.21
”	10 520	6.0664	2.511	−0.29	0.07	−0.01	−0.14	0.00	0.03	−0.10	−0.36	8.48
”	10 000	6.1303	2.849	−0.30	0.12	0.02	−0.06	0.03	0.04	−0.10	−0.26	8.77
”	9 500	6.1927	3.279	−0.33	0.16	0.05	0.06	0.06	0.06	−0.10	−0.20	9.08
”	9 050	6.2590	3.974	−0.36	0.19	0.09	0.18	0.09	0.07	−0.09	−0.16	9.42
”	8 660	6.3336	5.723	−0.39	0.22	0.12	0.30	0.12	0.09	−0.08	−0.14	9.78
”	8 230	6.3987	8.461	−0.42	0.26	0.15	0.44	0.15	0.12	−0.07	−0.12	10.14
”	7 330	6.5018	15.655	−0.45	0.34	0.23	0.77	0.23	0.17	−0.04	−0.10	10.88
”	6 880	6.5439	20.326	−0.42	0.40	0.26	0.95	0.27	0.20	−0.02	−0.09	11.26
0.230	30 010	6.4188	0.203	−1.06	−0.27	−0.13	−0.94	−0.17	−0.10	−0.17	−2.98	7.12
”	28 220	6.4678	0.203	−1.02	−0.25	−0.13	−0.90	−0.16	−0.10	−0.17	−2.84	7.37
”	26 430	6.5134	0.203	−0.99	−0.23	−0.12	−0.86	−0.15	−0.09	−0.16	−2.68	7.61
”	25 000	6.5480	0.203	−0.96	−0.22	−0.12	−0.82	−0.15	−0.08	−0.15	−2.54	7.80
”	23 350	6.5868	0.203	−0.92	−0.20	−0.11	−0.78	−0.14	−0.07	−0.15	−2.36	8.02
”	22 030	6.6168	0.204	−0.89	−0.19	−0.10	−0.74	−0.13	−0.07	−0.15	−2.21	8.19
”	20 710	6.6461	0.205	−0.85	−0.17	−0.10	−0.70	−0.12	−0.06	−0.14	−2.05	8.37
”	19 200	6.6727	0.214	−0.79	−0.15	−0.09	−0.65	−0.11	−0.05	−0.14	−1.85	8.56
”	17 860	6.6782	0.251	−0.74	−0.13	−0.09	−0.61	−0.10	−0.04	−0.13	−1.66	8.70
”	16 620	6.6907	0.299	−0.69	−0.10	−0.08	−0.56	−0.09	−0.04	−0.13	−1.47	8.85
”	15 380	6.7116	0.345	−0.62	−0.08	−0.07	−0.50	−0.08	−0.03	−0.13	−1.26	9.04
”	14 310	6.7331	0.390	−0.56	−0.05	−0.07	−0.45	−0.07	−0.02	−0.12	−1.07	9.21
”	13 320	6.7549	0.442	−0.50	−0.02	−0.06	−0.39	−0.06	−0.01	−0.12	−0.89	9.40
”	12 400	6.7768	0.501	−0.44	0.02	−0.05	−0.33	−0.04	0.01	−0.12	−0.71	9.59
”	11 530	6.7990	0.570	−0.40	0.06	−0.03	−0.25	−0.02	0.02	−0.11	−0.55	9.79
”	10 730	6.8210	0.648	−0.40	0.11	0.00	−0.15	0.01	0.03	−0.11	−0.38	9.99
”	9 910	6.8455	0.751	−0.41	0.15	0.04	0.00	0.05	0.05	−0.10	−0.26	10.28
”	9 220	6.8699	0.868	−0.44	0.20	0.09	0.17	0.09	0.07	−0.09	−0.20	10.59
”	8 600	6.8939	1.015	−0.47	0.24	0.13	0.35	0.14	0.10	−0.08	−0.16	10.91
”	8 070	6.9151	1.193	−0.48	0.28	0.17	0.51	0.17	0.13	−0.06	−0.13	11.21
”	7 000	6.9588	1.824	−0.46	0.38	0.25	0.90	0.26	0.20	−0.03	−0.10	11.91
”	6 460	6.9796	2.341	−0.40	0.45	0.30	1.13	0.30	0.24	−0.01	−0.10	12.31
”	5 970	6.9984	2.930	−0.31	0.54	0.36	1.37	0.36	0.27	0.02	−0.12	12.71
”	5 150	7.0477	4.075	−0.09	0.74	0.47	1.86	0.47	0.32	0.08	−0.23	13.59
”	4 810	7.0820	4.780	0.02	0.83	0.54	2.11	0.53	0.35	0.10	−0.32	14.07
”	4 460	7.1098	5.792	0.14	0.93	0.60	2.29	0.60	0.35	0.06	−0.43	14.58
”	4 110	7.1265	6.876	0.24	1.02	0.66	2.23	0.66	0.18	0.00	−0.49	15.04
”	3 780	7.1369	7.948	0.32	1.09	0.70	1.85	0.69	−0.08	−0.11	−0.46	15.39
”	3 450	7.1443	9.157	0.39	1.15	0.73	1.25	0.69	−0.27	−0.26	−0.35	15.69
”	3 210	7.1486	10.232	0.46	1.20	0.74	0.74	0.64	−0.36	−0.35	−0.22	15.89
”	2 980	7.1522	11.469	0.52	1.25	0.72	0.27	0.51	−0.38	−0.43	−0.07	16.07
”	2 760	7.1552	12.897	0.59	1.29	0.69	−0.16	0.33	−0.36	−0.54	0.08	16.26
”	2 530	7.1593	15.744	0.68	1.35	0.62	−0.70	0.04	−0.29	−0.69	0.26	16.46
”	2 310	7.1624	18.216	0.78	1.40	0.55	−1.27	−0.34	−0.20	−0.87	0.45	16.69
0.336	21 420	7.1810	0.045	−0.88	−0.16	−0.10	−0.73	−0.12	−0.06	−0.14	−2.13	9.22
”	19 620	7.1907	0.049	−0.82	−0.13	−0.10	−0.67	−0.11	−0.05	−0.14	−1.90	9.40
”	18 260	7.1978	0.065	−0.78	−0.11	−0.09	−0.62	−0.10	−0.05	−0.14	−1.71	9.54
”	17 010	7.2109	0.090	−0.72	−0.09	−0.08	−0.58	−0.09	−0.04	−0.13	−1.52	9.69
”	15 840	7.2270	0.121	−0.67	−0.06	−0.08	−0.53	−0.08	−0.03	−0.13	−1.33	9.85
”	14 640	7.2464	0.161	−0.61	−0.03	−0.07	−0.47	−0.07	−0.02	−0.12	−1.12	10.03
”	13 540	7.2658	0.210	−0.55	0.01	−0.06	−0.41	−0.06	−0.01	−0.12	−0.92	10.22
”	12 620	7.2830	0.268	−0.50	0.05	−0.05	−0.34	−0.04	0.01	−0.12	−0.75	10.40
”	11 810	7.2986	0.337	−0.48	0.08	−0.03	−0.27	−0.02	0.01	−0.12	−0.59	10.56
”	10 880	7.3163	0.445	−0.48	0.12	0.00	−0.16	0.01	0.03	−0.11	−0.41	10.78
”	10 020	7.3328	0.582	−0.48	0.16	0.05	0.00	0.06	0.05	−0.10	−0.29	11.06
”	9 370	7.3454	0.719	−0.50	0.20	0.09	0.16	0.09	0.07	−0.09	−0.23	11.33
”	8 720	7.3573	0.889	−0.52	0.23	0.13	0.33	0.13	0.10	−0.08	−0.18	11.62
”	8 120	7.3681	1.092	−0.52	0.27	0.17	0.51	0.17	0.13	−0.06	−0.15	11.93

Table 3 – *continued*

$M_*/M_\odot$	$T_{\rm eff}$	Log (g)	Age (Gyr)	$U-B$	$B-V$	$V-R$	$V-K$	$R-I$	$J-H$	$H-K$	BC	M_V
”	7 460	7.3795	1.370	−0.51	0.33	0.22	0.73	0.22	0.17	−0.04	−0.12	12.29
”	6 950	7.3883	1.640	−0.47	0.39	0.26	0.93	0.26	0.20	−0.03	−0.11	12.61
”	6 390	7.3987	2.023	−0.40	0.47	0.31	1.17	0.31	0.24	0.00	−0.11	13.00
”	5 870	7.4099	2.492	−0.29	0.56	0.37	1.43	0.37	0.28	0.03	−0.13	13.41
”	5 000	7.4416	3.926	−0.05	0.77	0.50	1.96	0.50	0.34	0.08	−0.26	14.32
”	4 610	7.4569	5.361	0.07	0.88	0.57	2.18	0.57	0.35	0.06	−0.38	14.83
”	4 240	7.4669	6.985	0.18	0.97	0.63	2.16	0.63	0.20	−0.01	−0.44	15.29
”	3 890	7.4727	8.597	0.26	1.05	0.68	1.80	0.67	−0.08	−0.10	−0.42	15.65
”	3 610	7.4760	9.997	0.32	1.10	0.70	1.28	0.68	−0.26	−0.25	−0.34	15.90
”	3 300	7.4790	11.832	0.40	1.16	0.72	0.76	0.64	−0.36	−0.34	−0.21	16.17
”	3 020	7.4813	14.033	0.47	1.21	0.70	0.22	0.51	−0.39	−0.43	−0.05	16.39
0.449	36 370	7.2604	0.002	−1.16	−0.28	−0.14	−1.00	−0.18	−0.12	−0.17	−3.45	8.13
”	34 060	7.2999	0.004	−1.13	−0.27	−0.14	−0.99	−0.18	−0.11	−0.17	−3.27	8.34
”	32 270	7.3577	0.011	−1.11	−0.26	−0.14	−0.97	−0.17	−0.11	−0.17	−3.13	8.58
”	30 310	7.4037	0.023	−1.09	−0.25	−0.13	−0.94	−0.17	−0.10	−0.17	−2.98	8.82
”	28 220	7.4342	0.035	−1.05	−0.23	−0.13	−0.90	−0.16	−0.10	−0.17	−2.82	9.04
”	26 220	7.4605	0.049	−1.01	−0.21	−0.12	−0.86	−0.15	−0.09	−0.16	−2.64	9.24
”	24 310	7.4844	0.068	−0.97	−0.19	−0.12	−0.81	−0.14	−0.08	−0.15	−2.45	9.44
”	22 530	7.5065	0.093	−0.93	−0.16	−0.11	−0.76	−0.13	−0.07	−0.15	−2.25	9.63
”	20 860	7.5270	0.128	−0.88	−0.14	−0.10	−0.71	−0.12	−0.06	−0.14	−2.05	9.81
”	19 290	7.5462	0.174	−0.83	−0.11	−0.10	−0.66	−0.11	−0.05	−0.14	−1.84	9.99
”	17 830	7.5638	0.237	−0.78	−0.09	−0.09	−0.61	−0.10	−0.04	−0.14	−1.63	10.17
”	16 470	7.5796	0.320	−0.72	−0.06	−0.08	−0.56	−0.09	−0.03	−0.13	−1.42	10.34
”	15 200	7.5938	0.429	−0.66	−0.02	−0.07	−0.50	−0.07	−0.02	−0.13	−1.21	10.51
”	14 030	7.6063	0.570	−0.60	0.01	−0.07	−0.44	−0.06	−0.01	−0.12	−1.00	10.69
”	12 920	7.6173	0.749	−0.55	0.06	−0.05	−0.36	−0.04	0.00	−0.12	−0.80	10.87
”	11 890	7.6273	0.982	−0.54	0.09	−0.03	−0.28	−0.02	0.01	−0.12	−0.59	11.04
”	10 910	7.6365	1.289	−0.53	0.13	0.01	−0.15	0.02	0.03	−0.11	−0.41	11.26
”	10 030	7.6452	1.672	−0.53	0.17	0.05	0.02	0.06	0.05	−0.10	−0.30	11.54
”	9 220	7.6532	2.148	−0.54	0.21	0.10	0.21	0.11	0.08	−0.09	−0.23	11.85
”	8 460	7.6606	2.728	−0.55	0.25	0.15	0.41	0.15	0.11	−0.07	−0.18	12.19
”	7 770	7.6674	3.349	−0.54	0.30	0.20	0.63	0.20	0.15	−0.05	−0.14	12.54
”	7 130	7.6741	3.969	−0.49	0.36	0.24	0.86	0.25	0.19	−0.03	−0.12	12.91
”	6 540	7.6806	4.611	−0.42	0.44	0.30	1.10	0.30	0.23	−0.01	−0.10	13.28
”	6 020	7.6874	5.330	−0.32	0.54	0.35	1.34	0.35	0.26	0.02	−0.12	13.67
”	5 540	7.6959	6.189	−0.21	0.63	0.41	1.59	0.41	0.29	0.05	−0.14	14.07
”	5 110	7.7067	7.472	−0.09	0.74	0.48	1.88	0.48	0.33	0.07	−0.24	14.55
”	4 710	7.7160	9.455	0.04	0.85	0.55	2.10	0.55	0.34	0.05	−0.34	15.04
”	4 330	7.7221	11.582	0.14	0.94	0.61	2.10	0.61	0.20	−0.01	−0.41	15.49
”	3 970	7.7258	13.651	0.22	1.02	0.66	1.79	0.65	−0.06	−0.09	−0.40	15.85
”	3 640	7.7282	15.838	0.30	1.08	0.69	1.19	0.66	−0.28	−0.26	−0.31	16.16

Ages are counted from the end of mass transfer.

becomes $\approx 0.18\ M_\odot$; see Althaus et al. 2001a). In addition, CNO flashes become less intense as the metal content of the star is decreased and the mass range for the occurrence of such instabilities depends strongly on the inclusion of chemical diffusion processes in evolutionary calculations. We also find that the existence of a mass threshold for the occurrence of diffusion-induced CNO flashes leads to an age dichotomy (particularly for $Z = 0.001$) between He WD models with and without CNO thermonuclear flashes: He WDs that do not experience CNO thermonuclear flashes evolve very slowly, so they remain relatively bright even at very large ages, whilst those that suffer from such flashes are characterized by a fast cooling, reaching very low effective temperature stages within cooling times less than 15 Gyr. Such an age dichotomy is translated into distinctive features in the isochrone plots that could eventually be compared with observational expectations. It is worth mentioning that during the short-lived, CNO diffusion-induced flashes, an appreciable amount of hydrogen is burnt, ultimately implying that the WD is left with a relatively thin hydrogen envelope that prevents stable hydrogen burning from being an important energy source at late cooling stages. As a result, the star has a much lower amount of available energy, which implies much shorter evolutionary time-scales compared with the situation when CNO flashes are absent.

Another finding of this work is related to the fact that some of our He WD models experience several episodes of thermal instabilities related to unstable hydrogen burning via the proton–proton nuclear reactions. These PP flashes, which take place at more advanced stages of evolution than those at which the CNO flashes occur, are experienced by all of our sequences with $Z = 0.0002$. In addition, our 0.172- and 0.183-$M_\odot$ models with $Z = 0.001$ suffer from PP flashes, but at exceedingly high ages. We find that PP thermal instabilities are triggered by chemical diffusion that carries some hydrogen downwards deep enough for the star to ignite hydrogen there. Except for the less massive models ($M \lesssim 0.25\ M_\odot$), PP flashes take place between 2 and 4 Gyr after the end of mass-loss episodes, and in general, the more massive the He WD, the earlier in the life of the star they occur.

The evolution of our He WD models has also been analysed in the colour–magnitude diagrams. We find that models that have suffered from CNO flashes exhibit a turn-off in most of their colours at $M_V \approx 16$. This turn-off, which results from the strong CIA opacity by molecular hydrogen at low temperatures, is reached well within 15 Gyr, mostly by He WDs with $Z = 0.001$. Finally, the predictions of our models for the colour–magnitude diagrams have been compared with recent observational data of He WD candidates in the globular clusters NGC 6397 and 47 Tucanae (Taylor et al. 2001; Edmonds et al. 2001, respectively). In this connection, we find that the three brightest He WD candidates in NGC 6397 can indeed be identified as He WDs characterized by stellar mass values of 0.20–0.22 $M_\odot$ (which is below the mass value for the occurrence of CNO flashes) and ages ranging from 0.5 to 1.5 Gyr. However, in the case of the three dimmest candidates, the agreement with observational data is not as evident as in the case of the brightest objects. Indeed, our models appear to be more massive than required by observations. Specifically, our mass-loss treatment gives rise to a minimum value of $\sim$0.2 $M_\odot$ an He WD may have from progenitors with initially $Z = 0.0002$. However, it is worth noting that a $\Delta(V - I) \approx 0.1$ would allow a very good agreement between theoretical predictions and observations. In this sense, it is remarkable that the quoted uncertainty in the case of the He WD candidate in 47 Tucanae is very close to this value (see Fig. 10).[3] Finally, the He WD in 47 Tucanae is particularly relevant because the spin-down age of its millisecond pulsar companion yields a WD age estimate. Specifically, the pulsar age of 2 Gyr (see Edmonds et al. 2001) is in agreement with the prediction of our $Z = 0.001$ He WD sequences. In addition, the observational data for M_V and $U - V$ is consistent with our 0.17-$M_\odot$ sequence.

Complete tables containing the results of the present calculations are available at http://www.fcaglp.unlp.edu.ar/evolgroup/ or upon request from the authors at their e-mail addresses.

REFERENCES

Althaus L.G., Serenelli A.M., Benvenuto O.G., 2001a, MNRAS, 323, 471
Althaus L.G., Serenelli A.M., Benvenuto O.G., 2001b, MNRAS, 324, 617
Anderson S.F., Margon B., Deutsch E.W., Downes R.A., Allen R.G., 1997, ApJ, 482, L69
Anthony-Twarog B.J., Twarog B.A., 2000, AJ, 120, 3111
Benvenuto O.G., Althaus L.G., 1998, MNRAS, 293, 177
Bergeron P., Saffer R.A., Liebert J., 1992, ApJ, 394, 228
Bergeron P., Ruiz M.T., Leggett S.K., 1997, ApJS, 108, 339
Bessell M.S., 1990, PASP, 102, 1181
Bessell M.S., Brett J.M., 1988, PASP, 100, 1134
Borysow A., Jorgensen U.G., Fu Y., 2001, JQSRT, 68, 235
Bragaglia A., Greggio L., Renzini A., D'Odorico S., 1990, ApJ, 365, L13
Bragaglia A., Renzini A., Bergeron P., 1995, ApJ, 443, 735
Burderi L., D'Antona F., Burgay M., 2002, ApJ, 574, 325
Burgers J.M., 1969, Flow Equations for Composite Gases. New York, Academic
Cool A.M., Grindlay J.E., Cohn H.N., Lugger P.M., Bailyn C.D., 1998, ApJ, 508, L75
Däppen W., Anderson L., Mihalas D., 1987, ApJ, 319, 195
Driebe T., Schönberner D., Blöcker T., Herwig F., 1998, A&A, 339, 123
Driebe T., Blöcker T., Schönberner D., Herwig F., 1999, A&A, 350, 89
Edmonds P.D., Grindlay J.E., Cool A.M., Cohn H.N., Lugger P.M., Bailyn C.D., 1999, ApJ, 516, 250
Edmonds P.D., Gilliland R.L., Heinke C.O., Grindlay J.E., Camilo F., 2001, ApJ, 557, L57
Eggleton P.P., 1983, ApJ, 268, 368
Gustafsson M., Frommhold L., 2001, ApJ, 546, 1168
Han Z., 1998, MNRAS, 296, 1019
Hansen B.M.S., Phinney E.S., 1998, MNRAS, 294, 557
Holtzman J.A., Burrows C.J., Casertano S., Hester J.J., Trauger J.T., Watson A.M., Worthey G., 1995, PASP, 107, 1065
Hummer D.G., Mihalas D., 1988, ApJ, 331, 794
Iglesias C.A., Rogers F.J., 1996, ApJ, 464, 943
Jorgensen U.G., Hammer D., Borysow A., Falkesgaard J., 2000, A&A, 361, 283
Kippenhahn R., Weigert A., 1990, Stellar Structure and Evolution, A&A Library. Springer-Verlag, Berlin
Kurucz R.L., 1979, ApJS, 40, 1
Landsman W., Aparicio J., Bergeron P., Di Stefano R., Stecher T.P., 1997, ApJ, 481, L93
Landau L.D., Lifshitz E.M., 1971, Classical Theory of Fields. Pergamon Press, Oxford
Lundgren S.C., Cordes J.M., Foster R.S., Wolszczan A., Camilo F., 1996, ApJ, 458, L33
Marsh T.R., 1995, MNRAS, 275, L1
Marsh T.R., Dhillon V.S., Duck S.R., 1995, MNRAS, 275, 828
Moran C., Marsh T.R., Bragaglia A., 1997, MNRAS, 288, 538
Orosz J.A., Wade R.A., Harlow J.J.B., Thorstensen J.R., Taylor C.J., Eracleous M., 1999, AJ, 117, 1598
Podsiadlowski Ph., Joss P.C., Hsu J.J.L., 1992, ApJ, 391, 246
Rohrmann R.D., 2001, MNRAS, 323, 699
Rohrmann R.D., Serenelli A.M., Althaus L.G., Benvenuto O.G., 2002, MNRAS, 335, 499
Saffer R.A., Livio M., Yungelson L.R., 1998, ApJ, 504, 392
Sarna M.J., Ergma E., Antipova J., 2000, MNRAS, 316, 84
Serenelli A.M., Althaus L.G., Rohrmann R.D., Benvenuto O.G., 2001, MNRAS, 325, 607
Taylor J.M., Grindlay J.E., Edmonds P.D., Cool A.M., 2001, ApJ, 553, L169
Townsley D.M., Bildsten L., 2002, ApJ, 565, L35
van Kerkwijk M.H., Bell J.F., Kaspi V.M., Kulkarni S.R., 2000, ApJ, 530, L37
Zoccali M. et al., 2001, ApJ, 553, 733

[3] It is worth mentioning that Townsley & Bildsten (2002) have recently suggested that the three dimmest He WD candidates in NGC 6397 could be cataclysmic variables involving a hot C-O WD and a low-mass main-sequence companion.

This paper has been typeset from a TEX/LATEX file prepared by the author.